Earthq Eng & Eng Vib (2009) 8:179-188 **DOI**: 10.1007/s11803-009-8139-z

Attenuation of peak ground accelerations from the great Wenchuan earthquake

Wang Dong[1†] and Xie Lili[1,2‡]

1. *Institute of Engineering Mechanics, China Earthquake Administration, Harbin 150080, China*
2. *School of Civil Engineering and Architecture, Harbin Institute of Technology, Harbin 150090, China*

Abstract: Over 800 accelerograms recorded by 272 ground-level stations during the Wenchuan earthquake are used to analyze the influence of rupture distance, local site conditions and azimuth on peak ground accelerations (PGAs). To achieve a better understanding of the characteristics of ground motions, the spatial distributions of the EW, NS and UD components of PGAs are obtained. Comparisons between the EW and NS components, the fault-normal and fault-parallel components, and the vertical and horizontal components of PGAs are performed, and the regression formula of the vertical-to-horizontal ratio of PGAs is developed. The attenuation relationship of peak horizontal accelerations (PHAs) is compared with several contemporary attenuation relationships. In addition, an analysis of residuals is conducted to identify the potential effects of rupture distance, azimuth and site conditions on the observed values of PHAs. The analysis focuses on medium-hard soil site conditions, as they provided most of the data used in this study.

Keywords: Wenchuan earthquake; peak ground acceleration (PGA); attenuation; rupture distance; azimuth

1 Introduction

In the afternoon (14:28:04, Beijing time) of May 12, 2008, an M 8.0 earthquake suddenly struck Wenchuan County of eastern Sichuan in China. The great Wenchuan earthquake with the characteristics of wide affected region, strong destructive effect and high economic losses, is believed to be the most devastating one struck China mainland ever since the great 1976 Tangshan earthquake. It was felt almost throughout China except in Heilongjiang, Xinjiang and Jilin provinces, and in parts of Bangladesh, India, Japan, Mongolia, Nepal, Pakistan, Russia, Thailand and Vietnam. At least 69,000 people were killed, 18,000 were missing and 37,000 were injured by the earthquake, and direct economic losses were estimated to be 845.1 billion (RMB) according to Zhongxinnet (http://www.chinanews.com.cn/gn/news/2008/09-04/1371101.shtml, last accessed on Nov. 16, 2008). An estimated 5.36 million buildings collapsed and more than 21 million buildings were damaged in Sichuan and in parts of Chongqing City, Gansu, Hubei, Shaanxi and Yunnan provinces. Fortunately, the China Digital Strong Motion Observation Network was brought into regular service in March, 2008 just before the great Wenchuan earthquake. During the major shock of this event, over 1,400 components of acceleration records were obtained from 460 permanent free-field stations and three observation arrays located throughout the Chinese mainland (Li *et al.*, 2008). Both the quantity and quality of the records are unprecedented in the history of Chinese strong motion observations, providing a great opportunity to study the characteristics of ground motions in severe earthquakes.

In this article, a preliminary analysis of strong-motion data from the Wenchuan earthquake is presented, focusing on attenuation characteristics, geological effects, and azimuth dependence of the peak horizontal accelerations (PHAs), a_{PH}, during the earthquake. One of most important issues is whether or not serious damage was caused by the strong ground motions. To answer this question, the available recordings were compared with ground-shaking amplitudes predicted by contemporary attenuation relationships from around the world.

2 Seismological data

The seismological data used in this article was obtained from a report released shortly after the earthquake by the U.S. Geological Survey (USGS, 2008). Although more information about the earthquake will be available after this study, the results presented

Correspondence to: Wang Dong, Institute of Engineering Mechanics, China Earthquake Administration, 9 Xuefu Road, Harbin 150080, China
Email:wangdong_iem@163.com
†PhD Candidate; ‡Professor

Supported by: National Natural Science Foundation of China Under Grant No. 90715038, 50878199 and 50808166; National Basic Research Program of China Under Grant No. 2007CB714200
Received November 20, 2008; **Accepted** December 23, 2008

herein will not significantly change.

According to the USGS (2008), the Wenchuan earthquake occurred at 06:28:01 UTC on May 12, 2008 (14:28:01, Beijing time) in Wenchuan County. Its hypocenter was located at 30.986°N latitude and 103.364°E longitude approximately 80 km west-northwest of Chengdu City at a depth of 19 km. A focal-mechanism solution (Chen and Gavin Hayes, 2008) was derived from several teleseismic broadband waveforms recorded by NEIC shortly after the event. The fault plane is defined as an inclined fault that strikes 229º and dips 33º northwest and is approximately 40 km wide (down-dip direction) by 320 km long (strike-parallel direction), which released a seismic moment of 0.115E+22 N·m. The surface projection of the finite-fault plane is shown in Fig. 1, where the black rectangle indicates the major plate boundary.

3 Strong-motion data

Shortly after this event, an intensive effort was made to make the data available for use by seismologists and engineers in the Seismological Bureaus of the provinces of Sichuan, Gansu, Shaanxi, and the China Strong Motion Net Center (CSMNC). More than 1,400 accelerograms were recorded from 460 permanent free field stations and three arrays for topographical effects and structural response observations in this event (Li *et al.*, 2008). According to the quality of records, these data are classified before the analysis. The incomplete records, those with low signal-to-noise ratio, those with one of three components missing and those obtained by stations far from the fault were all discarded in this article. Therefore, 816 accelerograms obtained from 272 ground-level stations within the rupture distance of 1,000 km are used as database. Figure 1 plots the locations of some stations used in this study. The largest PGA (EW: 957.8 Gal, NS: 652.85 Gal and UD: 948.01 Gal) among all the recordings was recorded by the Wolong station located 22 km northwest of the epicenter. There are 120 observation stations with PGA larger than 100 Gal. The acceleration time-histories (EW) of 13 stations within the rupture distance of 20 km are also shown in Fig. 1, and their PGAs, a_{PG}, are labeled at the end of the time histories.

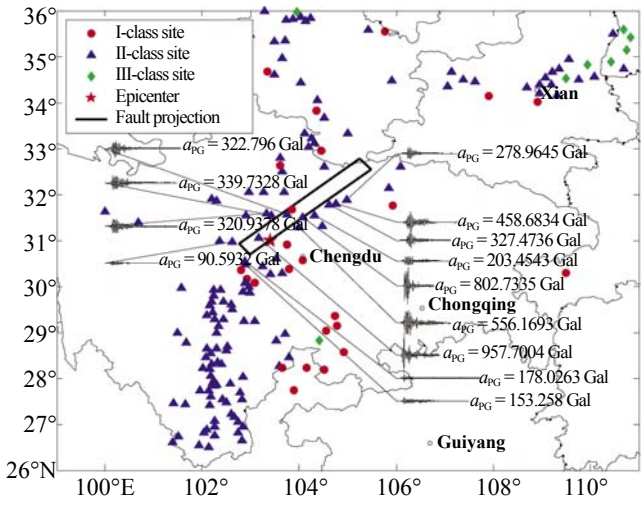

Fig. 1 Map showing the locations of some recordings used in this study

There are many definitions of the distance between the source and the site, such as the rupture distance D_{rup} (the closest distance from the site to the rupture surface), the seismogenic distance D_{seis} (the closest distance between the site and the seismogenic fault defined by Campbell in 1987), the epicentral distance and so on. In this article, the rupture distance is used as the source-to-site distance, and the reason is discussed below. The value of D_{rup} for each station used in this study is computed based on the finite-fault model (see Fig. 1, where the rectangle denotes the surface projection of the finite-fault) released on the webpage of USGS (USGS, 2008).

The classification of site conditions used in this study is shown in Table 1, which is based on the Chinese Seismic Design Code (GB 50011-2001). Based on the equivalent shear wave velocity V_{se} (i.e., the average shear wave velocity of the overlay soil) and the depth of the overlay soil H_{os}(i.e., the depth to the soil layer with shear wave velocity larger than 500 m/s), the site soils are classified into four categories: I- (rock or hard soil), II- (medium-hard soil), III- (medium-soft soil) and IV- class (soft soil). Among the 272 stations selected, the station numbers (percentage) are 36 (13.2%), 206 (75.7%) and 30 (11.0%) for site classes I, II and III, respectively; i.e., most are for stations on site class II and none are from site class IV.

Table 1 Classification of site condition based on the Chinese Seismic Design Code (GB 50011-2001)

Equivalent shear wave velocity (m/s)	Depth of overlay soil (m)			
	I-class	II-class	III–class	IV–class
V_{se}>500	0	---	---	---
500≥V_{se}>250	<5	≥5	---	---
250≥V_{se}>140	<3	3–50	>50	---
V_{se}≤140	<3	3–15	15–80	>80

The spatial distribution of ground motion amplitudes is very useful in understanding the characteristics of ground motions. The dense data recorded in this event made it possible to plot the distribution of PGAs in space. Figure 2 shows the contour maps of three-component PGA derived from the 816 accelerograms. Significant findings are as follows:

(1) No considerable difference as a whole is observed in the spatial distributions of the three-component PGAs except the amplitudes, especially the PGAs of two horizontal components.

(2) The spatial distributions of PGA in the near-fault

region are dominated by two records with high values of PGA at Wolong station in Wenchuan County and Qingping station in Mianzhu County, which produce "bulls eye" around these two data points. In addition, all the records over the vertical projection of rupture surface are located at the southwest part of the fault, and if there were several records obtained at the northeast part of fault, the contour lines with the EW component of PGA a_{EW}>350 Gal and the UD component of PGA a_{UD}>250 Gal should be obviously elongated toward northeast. Owing to the limited amount of the near-fault recordings (there are only few records over the projection of the fault surface, see figure 1), the contour maps herein can not accurately represent the spatial distribution of PGAs in the near-fault region and need further investigation.

(3) The isolines of the PGAs are obviously elongated along the strike-parallel direction, and the PGA attenuates as the rupture distance increases instead of the epicentral distance. Accordingly, the rupture distance is used as the source-to-site distance measure in this study.

(4) Caused by the hanging wall/footwall effect on the near-fault ground motion, the PGA attenuates slower on the hanging wall than on the footwall side in the near-fault region, while the attenuation rate of both sides tends to be uniform in the areas farther away from the fault.

(5) The affected region of strong motions (a_{PG} > 100 Gal, which is a meaningful value for engineering) is much larger in the forward direction of the rupture propagation (northeast) than in the backward direction (southwest). Furthermore, the PGAs in the forward direction of the rupture propagation attenuate much slower than those in the opposite direction. This is explained by the forward rupture directivity. Since the rupture began from the epicenter located near one edge of the fault and propagated unilaterally along the northwest strike, it met the conditions for generating forward rupture directivity effects.

4 Attenuation characteristics

4.1 Ground-motion model

To study the attenuation of ground motions, the

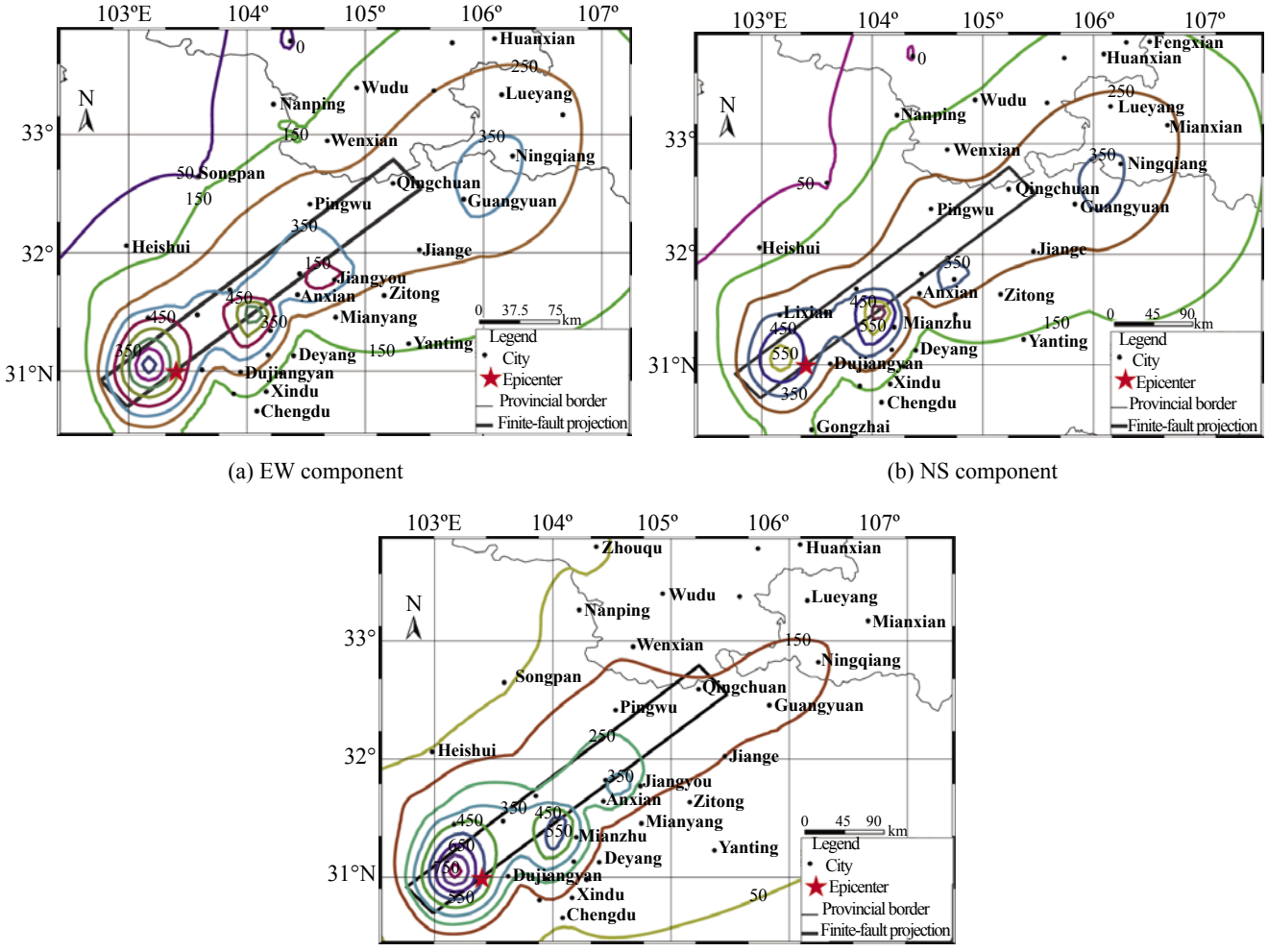

(a) EW component

(b) NS component

(c) UD component

Fig. 2 Contour maps of PGA (cm/s²) from the Wenchuan earthquake

attenuation model is expressed as follows:

$$\log_{10} Y = a + b \cdot \log_{10}(D_{\text{rup}} + c) \quad (1)$$

where Y denotes the PGA (cm/s^2); and D_{rup} is the closest distance to the rupture plane in kilometers; The parameters *a, b* and *c* are coefficients to be derived from the regression based on the least-squares method. Parameter *b* is used to accommodate both the geometric and inelastic attenuation. The regression parameters together with the standard deviation $\sigma_{\log_{10} Y}$ of the regression for different components from the 206 stations located on the medium-hard sites (II) are listed in Table 2. a_{PH} denotes the peak horizontal acceleration (PHA), which is defined as the geometric mean of the EW and NS components of PGAs, a_{EW} and a_{NS}.

Table 2 Regression coefficients for PGA from 206 stations on Site II in the Wenchuan earthquake

Component	*a*	*b*	*c*	$\sigma_{\log_{10} Y}$
a_{EW}	4.262	-1.171	11.250	0.310
a_{NS}	4.233	-1.159	12.649	0.311
a_{UD}	4.112	-1.223	7.916	0.268
a_{PH}	4.230	-1.158	11.540	0.306
a_{normal}	4.144	-1.126	9.577	0.312
a_{parallel}	4.263	-1.172	12.278	0.303

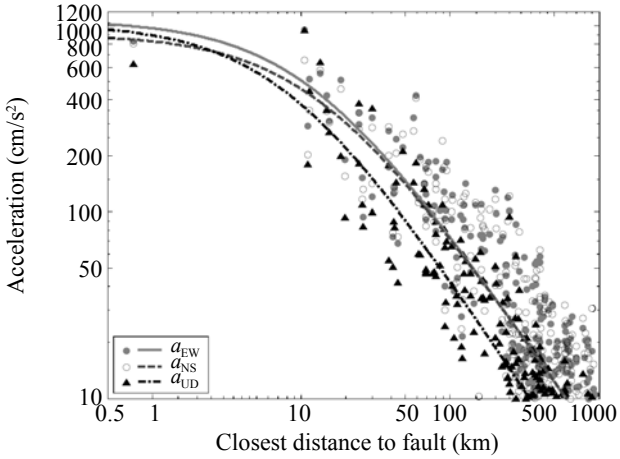

Fig. 3 Attenuation curves of PGAs (three components) from the Wenchuan earthquake (derived from 206 stations each with three-component recordings on Site II)

4.2 Attenuation comparisons

4.2.1 Comparison between EW and NS components

Figure 3 shows the PGA attenuations of the EW, NS and UD components, a_{EW}, a_{NS} and a_{UD}, for site class II, respectively, where the data from all the individual components are also illustrated. Note that there is no considerable difference between the PGAs of the EW and NS components except for rupture distances within about 15 km, but the two lines become almost the same beyond the distance of 20 km. In fact, the PGAs of the EW component are larger than the NS component by 10%–20% in the near-fault region. The number and percentage of stations with EW components greater than NS components in different distance ranges are listed in Table 3, and the mean and maximum ratios of $a_{\text{EW}} / a_{\text{NS}}$ are listed in Table 4. Note that in 88% of the nine near-source stations, the EW component is larger than the NS component. The average mean of ratio of $a_{\text{EW}} / a_{\text{NS}}$ within 20 km of the fault is much larger than in the other distance ranges.

4.2.2 Comparison between fault-normal and fault-parallel components

The large differences between the PGAs of the EW and NS components , a_{EW} and a_{NS}, discussed above suggest that it is important to compare the PGA of the fault-normal component, a_{normal}, with the fault-parallel component, a_{parallel}. As a matter of fact, it was found that the near-source PGAs of the fault-normal component are much larger than the fault-parallel component in previous earthquakes such as the 1992 Landers earthquake (Campbell and Bozorgnia., 1994), 1994 Northridge earthquake (Somerville *et al.,* 1997) and 1999 Chi-Chi earthquake (Wang GQ *et al.*, 2002). In this study, the two horizontal components of each selected accelerogram were rotated to fault-normal and fault-parallel orientations by means of an orthogonal coordinate transformation. Figure 4 plots the regression lines for both the fault-normal and fault-parallel components, and the corresponding regression coefficients are listed

Table 3 Number and percent of stations corresponding to peak ratio $\frac{a_{\text{EW}}}{a_{\text{NS}}} > 1$, $\frac{a_{\text{normal}}}{a_{\text{parallel}}} > 1$, and $\frac{a_{\text{V}}}{a_{\text{H}}} > 1$ in different distance ranges

Distance range (Number of recordings)	$a_{\text{EW}} / a_{\text{NS}} > 1$		$a_{\text{normal}}/a_{\text{parallel}}>1$		$a_{\text{V}}/a_{\text{H}}>1$	
	Number	Percent (%)	Number	Percent (%)	Number	Percent (%)
0–20 km (9)	8	88	4	44	3	33
20–50 km (14)	5	36	9	64	2	14
50–100 km (22)	16	72	7	32	0	0
100–200 km (25)	9	36	14	56	0	0
200–400 km (90)	48	53	43	47	4	0.04
≥ 400 km (112)	51	46	63	56	2	0.02

in Table 2, respectively. The fault-normal PGAs, a_{normal}, are slightly larger than the fault-parallel PGAs, $a_{parallel}$, by 10%–15% within a rupture distance of 10 km, while the two components become nearly the same as the rupture distance increases. This tendency can also be seen from the statistical data for the ratio of fault-normal to fault-parallel listed in Tables 3 and 4. This is due to the rupture directivity as shown in previous research (Somerville *et al.,* 1997), which demonstrated that this effect usually occurs in dip-slip earthquakes. The Wenchuan earthquake happened to occur on a dipping fault with dip-angle of 33º according to the focal mechanism given by USGS (Chen and Gavin Hayes, 2008). The propagation of the fault rupture towards a site at a velocity close to the shear wave velocity accumulates almost all of the seismic radiation from the dipping fault, causing the fault-normal PGAs to be larger than the fault-parallel ones.

4.2.3 Comparison between vertical and horizontal components

From Fig. 3, the PGAs of the vertical component are much less than the two horizontal components almost in all ranges of rupture distance except in the near-fault region, and the difference between the vertical and the two horizontal components decreases as the rupture distance increases. The PGAs of the vertical component are very close to or even larger than the NS component within a rupture distance of 10 km.

An attenuation relationship to fit the ratio of vertical to horizontal (a_V/a_H) for site class II of 202 stations, similar to Eq. (1), is developed as follows.

$$a_V/a_H = 0.902 - 0.137\log_{10}(D_{rup}+1) \quad (2)$$

where a_H denotes PHA. The corresponding regression curve is shown in Fig. 5, where the ratios for site classes I and III are also provided using different marks. Obviously, the a_V/a_H ratio decreases gradually as the rupture distance increases.

Table 4 presents a detailed comparison of the a_V/a_H ratio in different distance regions. Note that in the near-fault region (within rupture distance of 20 km), the mean and maximum value of the a_V/a_H ratio are 0.89 and 1.20, respectively. And 33% of the nine near-fault stations are the case that the vertical components are larger than the horizontal components, indicating that the near-fault PGAs of the vertical component are approximate to, or even larger than those of horizontal component. And, the a_V/a_H for six recordings (67%) are greater than 0.75, which is the value for the ratio of a_V/a_H recommended by the Chinese Seismic Design Code (GB 50011-2001).

Table 4 Mean and maximum values of $\frac{a_{EW}}{a_{NS}}$, $\frac{a_V}{a_H}$ and $\frac{a_{normal}}{a_{parallel}}$ in different distance ranges

Distance range (Number of recordings)	a_{EW}/a_{NS}		$a_{normal}/a_{parallel}$		a_V/a_H	
	Mean	Maximum	Mean	Maximum	Mean	Maximum
0–20 km (9)	1.15	1.48	1.02	1.51	0.89	1.20
20–50 km (14)	0.99	1.31	1.09	1.59	0.73	1.18
50–100 km (23)	1.05	1.42	0.93	1.41	0.54	0.93
100–200 km (25)	0.96	1.42	1.05	1.48	0.55	0.72
200–400 km (90)	1.08	3.93	1.02	1.64	0.59	1.33
≥ 400 km (112)	1.01	1.97	1.07	2.26	0.52	1.55

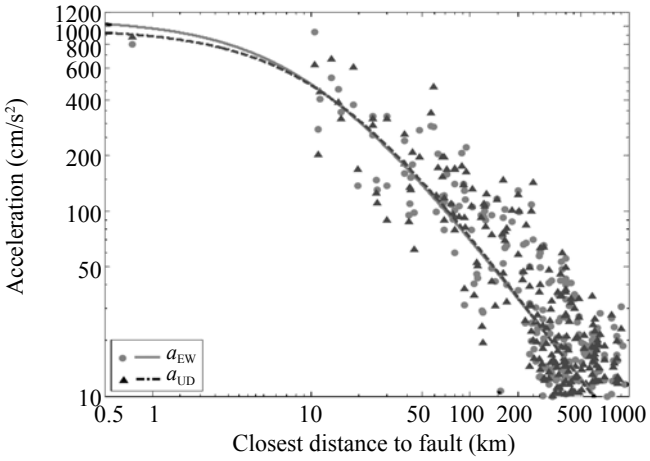

Fig. 4 Attenuation curves of PGA for fault-normal and fault-parallel components (derived from 206 stations each with three-component recordings on Site II)

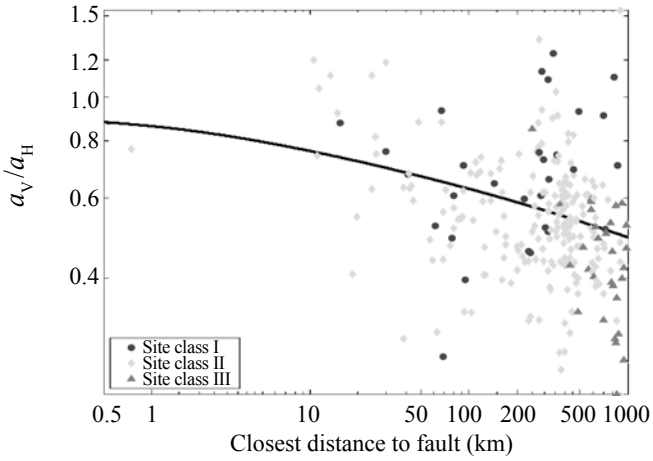

Fig. 5 Attenuation curve of ratio of vertical to horizontal PGAs (derived from 206 stations each with three-components on Site II)

In the region of rupture distances between 20–200 km, the mean a_V/a_H ratios vary in the range of 0.55–0.73, and the maximum a_V/a_H ratios vary in the range of 0.72–1.18. However, for regions with the rupture distances larger than 200 km, the corresponding ratios are 0.52–0.59 and 0.72–1.55. In addition, the mean and maximum values of the a_V/a_H ratios for regions with a rupture distance larger than 20 km are 0.55 and 1.54, respectively, which implies that the vertical PGAs are much less than the horizontal PGAs in the medium-far- and far-field regions. Note that the maximum values of a_V/a_H in distance ranges between 200–400 km and > 400 km are as high as 1.33 and 1.55, respectively, which seems to be questionable and needs field survey.

4.2.4 Comparison with the contemporary attenuation relationships

The Wenchuan-specific attenuation relationships of PHAs described in the preceding section are compared with contemporary attenuation relationships widely used in Southwest China (Huo, 1989), Chinese Taiwan (Loh *et al.*, 1998), Japan (Fukushima and Tanka, 1990) and the USA (Boore *et al.*, 1997). They are abbreviated in this study as China-89, Chinese Taiwan-98, Japan-90 and USA-97, respectively. Their formulas are listed in Table 5, where R denotes the shortest distance to the fault in kilometers; M is the moment magnitude; h in the last line is used in USA-99 as a fictitious depth to prevent a zero distance, and Vs (herein, it is assumed that V_s=250 m/s corresponding to the lower bound of velocity for medium-hard site according to USA-99) is the shear-wave velocity of the site. Note also that all these regression formulas corresponds to the soil sites, which are the majority of the recording sites in this event and the database used to develop the Wenchuan-specific attenuation relationships in this study. The PHAs regression curves for the Wenchuan earthquake and the empirical attenuation relationships mentioned above are shown in Fig. 6. Note that the PHAs in the

Table 5 Attenuation formulas and standard deviations of the contemporary attenuation relationships

Region	Attenuation formulas	Standard deviation	Unit of a_{PH}
China-89	$\log a_{PH} = 0.163+0.722M-1.842\log(R+0.125\exp(0.727M))$	0.339	g
Taiwan-98	$a_{PH} = 0.002968\exp(1.2M)(R+0.1464\exp(0.6981M))^{-1.7348}$	---	cm/s^2
Japan-90	$\log a_{PH} = 0.41M - \log(R + 0.032 \cdot 10^{0.41 \cdot M}) - 0.0034R + 1.3$	0.210	cm/s^2
USA-97	$\ln a_{PH} = -0.117 + 0.527(M - 6) - 0.778\ln(\sqrt{R^2 + h^2}) - 0.371\ln(V_s/1396)$	0.208	g

near-fault region approach to 1 g, which will greatly affect the buildings located a few kilometers from the earthquake rupture. In fact, from many historically major earthquakes, it is known that serious damage to structures is well correlated with high values of PHAs in the near-fault region, such as in the 1995 Kobe and 1999 Chi-Chi earthquakes. The severe damage to structures located very close to the fault resulted from unprecedented strong ground motions during these earthquakes. Similarly, the most affected areas in this event such as the County / Town Wenchuan, Jiangyou, Dujiangyan and Mianzhu are all located within the D_{rup} of 10 km. Such severe damage to structures in these regions are also believed to be caused by the extremely high ground motions.

The Chinese Taiwan-98 and Japan-90 underestimate the Wenchuan PHAs by 30%–40% and 50%–60% in near-fault region (<10 km) respectively, but slightly overestimate them for the medium-far and far distance range (20–200 km). China-89 basically provides a better estimation within few kilometers of rupture distance, although it greatly overestimates the PHAs by approximately 10%–40% in the medium-far and far distance of 20-200 km. Note that there is a large difference between USA-97 and the Wenchuan-specific relationship for PHA in almost all distance ranges.

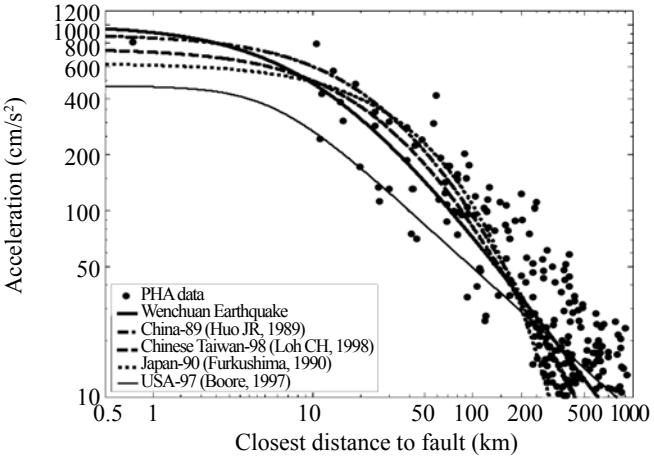

Fig. 6 Attenuation relationship of PHA for the Wenchuan earthquake (derived from 206 three-component recordings on Site II) compared to some other attenuation relationships developed previously

5 Residual analysis

An analysis of residuals is used to identify the potential effects of rupture distance, azimuth and site conditions on the observed values of PHAs. The residuals were computed with respect to Eq. (1) and normalized by $\sigma_{\log_{10} Y}$ resulting in the following:

$$R_{Ni} = (\log_{10} Y_i - \log_{10} Y) / \sigma_{\log_{10} Y} \quad (3)$$

where R_N is the normalized residual (RN); i is the index of recording; Y_i is the ith observed value of the PHA; Y is the predicted value; and $\sigma_{\log_{10} Y}$ is the standard error of regression.

The positive values of the R_{Ni} indicate that the recorded value is larger than the value predicted by the attenuation relationships; conversely, the negative R_{Ni} indicates that the recorded value is smaller than the predicted value. Since the residuals are normalized by $\sigma_{\log_{10} Y}$, a residual of ±1 represents a deviation of minus-and-plus one standard error between the recorded and predicted values of PHAs. If the residuals are supposed to be normally distributed, then R_N becomes a standard normal random variable. In this case, the normalized residuals of zero would correspond to a recording that falls at the 50th percentile (the median) of the distribution of residuals, and normalized residuals of -1 and +1 would correspond to the recordings that fall at the 16th percentile and 84th percentile of this distribution, respectively.

5.1 Influence of site-condition

Plots of the R_N versus the rupture distance for different site classes are displayed in Figs. 7(a), (b) and (c), respectively. Note that there is no visible trend for the residuals from site class II (see Fig. 7(b)), since the attenuation relationship has just been developed based on recordings at this site. However, there are obvious biases with respect to zero for the residuals of site classes I and III (see Fig. 7(a) and (c)). The residuals for rock sites are biased to negative in regions of moderate to far field, indicating that the rock sites encountered relatively lower PHAs than the medium-hard-soil sites in the Wenchuan earthquake. Conversely, the medium-soft sites appear to have larger PHAs than the medium-

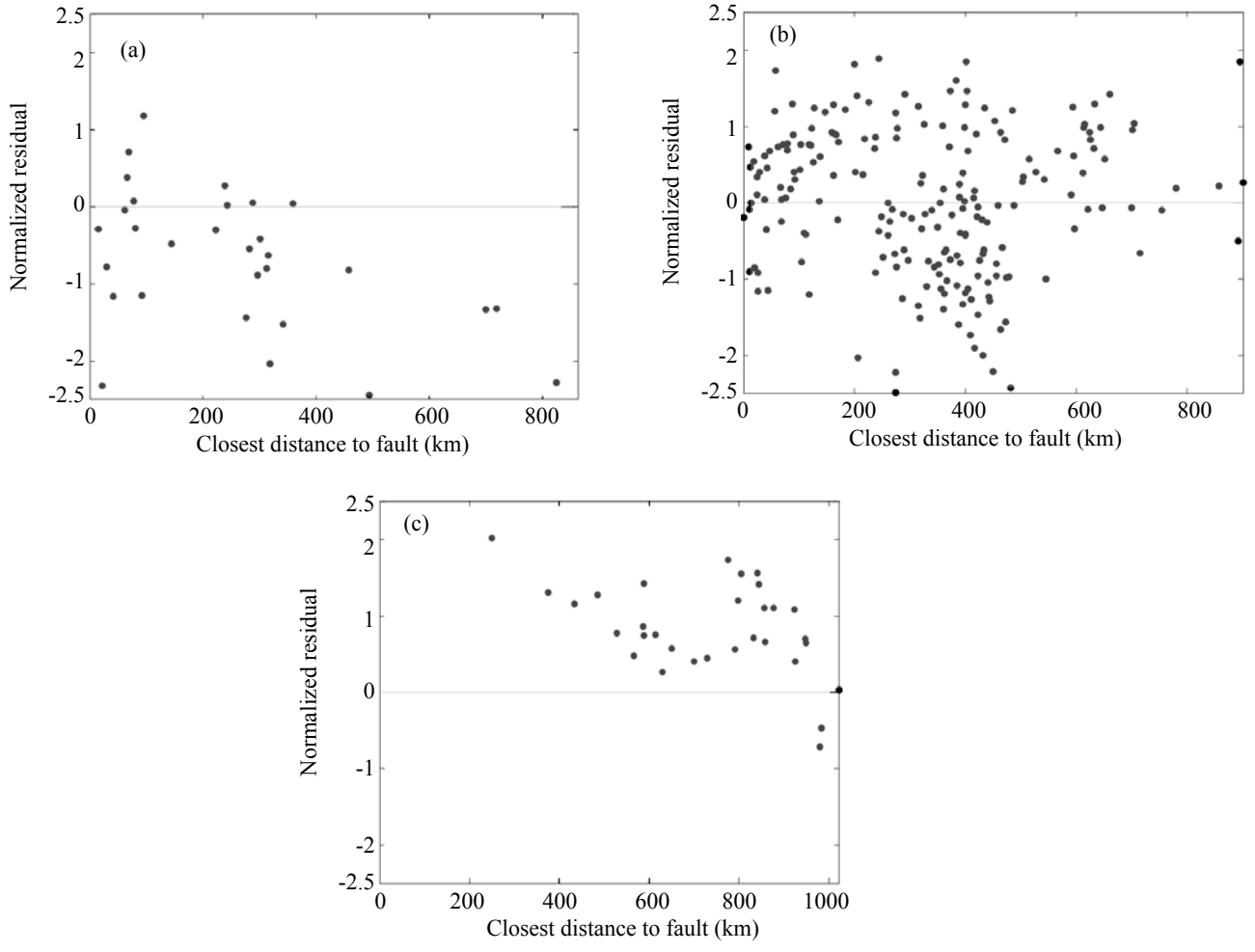

Fig. 7 Normalized residuals versus rupture distance for site classes I (a), II (b) and III (c)

Table 6 Summary of local site condition on the PHAs

Site class	Number of recordings	Mean of R_N ($\overline{R}_N$)	Standard deviation of R_N (σ_{R_N})	Site factor ($S = e^{\sigma \cdot \overline{R}_N}$)
I	36	-0.55	0.98	0.68
II	206	0	0.96	1
III	30	0.52	0.51	1.44

hard-soil sites in regions in the far-field with rupture distances larger than 200 km, since most of the residuals are located above the zero line. Similar features can be observed from Fig. 10.

To further identify the effects of site conditions on the ground motions, Table 6 summarizes the statistical characteristics of different sites. A site factor s defined as $s = \mathrm{Exp}(\sigma \cdot \overline{R}_N)$ is introduced (where $\overline{R}_N$ denotes the mean of R_N, and σ represents the regression deviation), i.e., the ratio of the median estimate of PHA for a given site classification to that of the medium-hard soil site. Since the attenuation relationship of PHA is derived from the data of 202 medium-hard sites, s = 1 for the medium-hard sites (see Table 6, $\overline{R}_N$ for medium-hard sites equals to zero), then compared to the medium-hard site, the rock site has a decreased PHA by 32% (s = 0.68), and the medium-soft site has an increased PHA by 44% (s =1.44). The effect of site conditions on the PHA from the Wenchuan earthquake is illustrated in Fig. 8, where a vertical error bar gives the median and one standard deviation estimate for each site factor.

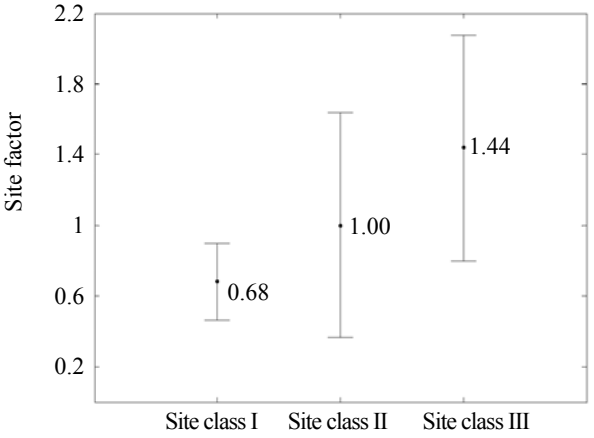

Fig. 8 Effect of site condition on PHAs from the Wenchuan earthquake

5.2 Influence of azimuth

The azimuth is defined as the angle between the true north and a vector drawn from the epicenter to the station, measured clockwise from north. Figure 9 displays a plot of azimuth versus rupture distance. Note that a distance greater than 300 km between azimuth of 240º and 320º and all distances between azimuth of 80º and 160º are not well represented by the recordings, which means that there may be an azimuth bias with respect to Eq. (1).

A plot of normalized residuals as a function of azimuth for different site conditions is shown in Fig. 10. The plot for medium-hard soil sites shows a tendency for relatively high PHAs at sites located northeast (azimuth of 20º to 80º) of the epicenter, and relatively small PHAs at sites located northwest and north of the epicenter (azimuth of 320º to 010º).

To identify the effect of azimuth on the ground motions, Table 7 summarizes the statistical characteristics of three azimuths: northeast (azimuth of 20º to 80º), northwest and north (320º to 10º) and all azimuths (0º to 360º). Similar to the influence of site conditions described above, if s is used as an azimuth factor, i.e., the ratio of the median estimate of PHA for sites located in a given azimuthal range to that for sites located at all azimuths, it is found that sites at azimuths of 20º to 80º had median

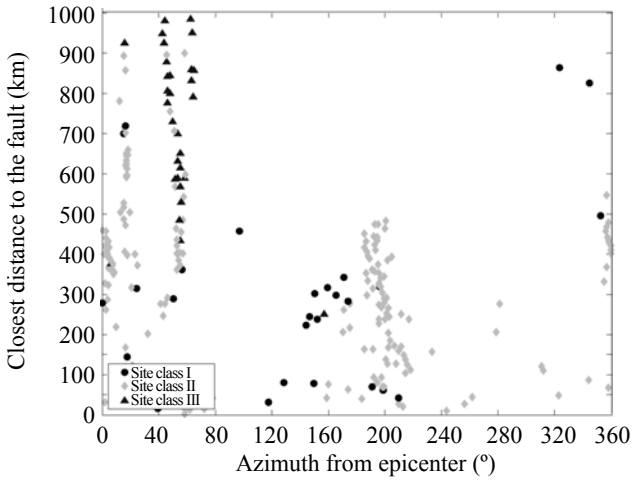

Fig. 9 Rupture distance versus azimuth for different sites

PHAs higher than 70% (s = 1.70), and sites at azimuths of 320º to 10º had median PHAs 36% (s=0.64) lower than sites located at all azimuths. The effect of azimuth on PHAs from the Wenchuan earthquake is shown in Fig. 11, where a vertical error bar gives the median and one standard deviation estimate for each azimuth range. The higher values of PHA toward the northeast are also consistent with the directivity resulting from the rupture propagation towards the northeast. The lower values of PHA towards northwest/north are somewhat of an anomaly and need further study.

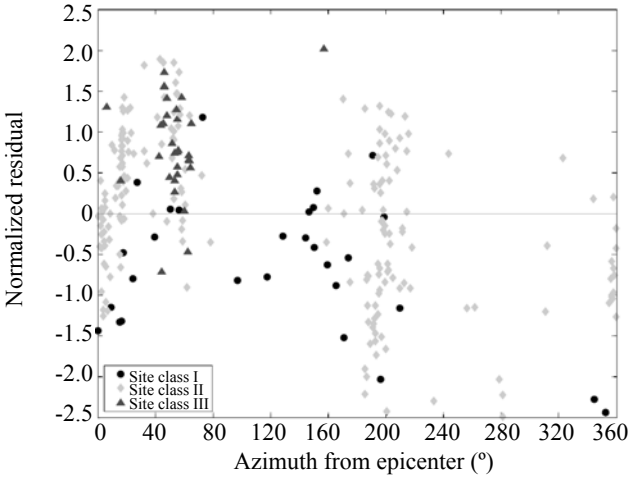

Fig. 10 Normalized residuals versus azimuth for different sites

6 Discussions and conclusions

Based on an empirical analysis of the peak ground acceleration (PGA) presented in this study, the following conclusions regarding the engineering characteristics of strong ground motions obtained during the Wenchuan earthquake can be drawn:

(1) The influence of various factors such as rupture process, local site conditions, propagation path, hanging wall/footwall effect, directivity effect and so on, on near-fault ground motions recorded during the Wenchuan earthquake are quite different from the far-field ground motions. First, the PGA of the fault-normal is larger than the fault-parallel component by 10%-15% in the near fault region (within 10-20 km to the fault), while they become almost the same as the rupture distance

Table 7 Summary of azimuth effect on the PHAs

Azimuth	Number of recordings	Mean of R_N ($\overline{R}_N$)	Standard deviation of R_N (σ_{R_N})	Azimuth factor ($S = e^{\sigma \cdot \overline{R}_N}$)
20º–80º	77	0.76	0.67	1.70
320º–10º	53	-0.64	0.81	0.64
0º–360º	206	0	1	1.00

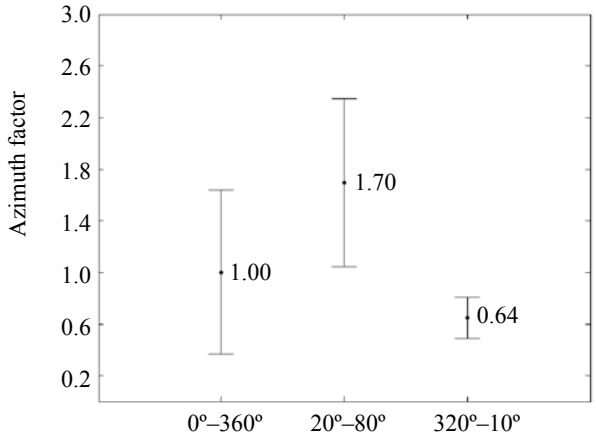

Fig. 11 Effect of azimuth on PHAs from the Wenchuan earthquake

increases. Second, the vertical PGA approaches, or even exceeds the horizontal PGA within a rupture distance of 20 km, and the difference between them decreases gradually as the distance increases.

(2) Both the horizontal and vertical components of PGAs from the Wenchuan earthquake attained 1 g within a few kilometers of the rupture, resulting in great damage to engineering structures in this region.

(3) The contemporary attenuation relationship widely used in Southeast China basically does a good job of predicting the Wenchuan earthquake PHAs within a rupture distance of 10 km, but it overestimates PHAs by approximately 10–40% in the distance range of 20–200 km.

(4) The ground motions from the Wenchuan earthquake are found to be significantly affected by local site conditions, and the attenuation relationship derived from the data recorded on medium-hard soil sites underestimated the PHAs by 32% for rock sites and overestimated by 44% for medium-soft sites.

(5) In the Wenchuan earthquake, the azimuth shows a significant influence on the ground motions. Recording stations located northeast of the epicenter (between 20º and 80º) were found to have accelerations approximately 70% higher and those located north and northwest of the epicenter (between 320º and 10º) were found to have accelerations 36% lower than those located at all azimuths (between 0º and 360º).

Note that this study was limited to the attenuation of PGAs from the Wenchuan earthquake. An analysis of the response spectral accelerations is more important for engineering structural analysis and design, and is currently being conducted.

Acknowledgment

We sincerely thank the people who installed and maintained the accelerographs. The authors express their gratitude to Prof. Yu Haiying for his kindness in

providing the recordings used in this study. We are also very grateful to the experts in the Seismological Bureaus of Provinces of Sichuan, Gansu, Shanxi, etc., for supplying the site conditions, and we would like to thank all who contributed to the success in recording, collecting and processing data in the Wenchuan Earthquake. We also gratefully acknowledge the constructive comments and suggestions of Wang Haiyun, Hu Jinjun, and the two anonymous reviewers.

References

Boore DM, Joyner WB and Thomas EF (1997), "Equations for Estimating Horizontal Response Spectra and Peak Acceleration from Western North American Earthquake: A Summary of Recent Work," *Seism. Res. Lett*., **1**: 128–153.

Campell KW (1991), "An Empirical Analysis of Peak Horizontal Acceleration for the Loma Prieta, California, Earthquake of 18 October 1989," *Bull. Seism. Soc. Am.*, **81**(5): 1838–1858.

Campell KW and Bozorgnia Y (1994), "Empirical Analysis of Strong Ground Motion from the 1992 Landers, California, Earthquake,". *Bull. Seism. Soc. Am.*, **84**: 573–588.

Chen Ji and Gavin Hayes (2008), "Finit Fault Model-Preliminary Result of the May 12, 2008 M_w 7.9 Eastern Sichuan, China earthquake," *Report by U.S.Geological Survey*,(http://earthquake.usgs.gov/eqcenter/eqinthenews/2008/us2008ryan/finitefault. php, lasted accessed Nov 16th, 2008).

China Ministry of Construction (2001), *Code for Seismic Design of Buildings* (GB 50011-2001), Beijing: China Construction Industry Printing House. (In Chinese)

Fukushima Y and Tanka T (1990), "A New Attenuation Relation for Peak Horizontal Acceleration of Strong Earthquake Ground Motion in Japan," *Bull. Seism. Soc. Am.*, **80**: 757–83.

Huo JR (1989), "Study on the attenuation laws of strong earthquake ground motion near the source," *PhD Dissertation*. Institute of Engineering Mechanics, China Earthquake Administration. (in Chinese)

Li XJ, Zhou ZH, Yu HY, Wen RZ, Lu DW, Huang M, Zhou YN and Cui JW (2008), "Strong Motion Observation and Recordings from the Great Wenchuan Earthquake," *Earthquake Engineering and Engineering Vibration*, **7**(3): 235–246.

Loh CH, Hwang CS and Jean YW (1998), "Seismic Demand Based on Damage Control Model-considering Basic Effect and Source Effect," *Soil Dyn. Earthquake Eng.*, **17**: 335–45.

Somerville PG, Smith NF, Graves RW and Abrahamson NA (1997), "Modification of Empirical Strong Ground Motion Attenuation Relations to Include the Amplitude and Duration Effects of Rupture Directivity," *Seism. Res. Lett*., **1**: 199–222.

USGS (2008), "Magnitude7.9, Eastern Sichuan, China," (http://earthquake.usgs.gov/eqcenter/recenteqsww/Quakes/us2008ryan.php, lasted accessed Nov 16th, 2008).

Wang GQ, Zhou XY, Zhang PZ and Igel H (2002), "Characteristics of Amplitude and Duration for Near Fault Strong Ground Motion from the 1999 Chi-Chi, Taiwan Earthquake," *Soil Dyn. Earthquake Eng*., **22**:73–94.